PAPER

Check for updates

Promoting the hydrogen evolution reaction through oxygen vacancies and phase transformation engineering on layered double hydroxide nanosheets†

Shujie Liu,[a] Jie Zhu,[a] Mao Sun,[a] Zhixue Ma,[a] Kan Hu,[a] Tomohiko Nakajima, [ID] *[b] Xianhu Liu, [ID] [c] Patrik Schmuki [ID] *[d] and Lei Wang [ID] *[ac]

In electrocatalysis, layered double hydroxide (LDH) materials have attracted considerable interest in promoting the oxygen evolution reaction (OER). For the hydrogen evolution reaction (HER), these materials show a poor electrocatalytic activity. In this work, we take CoFe LDH grown on nickel foam as a model system, and for the first time we treat CoFe LDH under plasma etching conditions, which results in a highly active HER electrocatalyst in alkaline media. Massive defects and amorphous phase formation occur during plasma etching. More importantly, phase transformation of CoFe LDH into $CoFe_2O_4$ takes place. Additional introduction of Ce leads to more active sites and improved electrical conductivity, which provide an overpotential of 73 mV at a current density of 10 mA cm^{-2} for V-Ce/CoFe LDH. The experimental results match well with DFT calculations, proving that defect engineering, phase transformation, and electronic structure tailoring can result in a high efficiency of HER activity. Moreover, a cell constructed of CoFe LDH||V-Ce/CoFe LDH is capable of overall water splitting with a cell voltage as low as 1.65 V at 10 mA cm^{-2} and a remarkable long-term stability of 60 h. The plasma etching strategy can also be effective for other LDH-based electrocatalysts (*e.g.* NiFe LDH and NiCo LDH), which demonstrates the universality of the strategy for improving HER performance. This work provides a simple but feasible pathway for designing alkaline HER electrocatalysts based on advanced LDH materials.

Introduction

Electrochemical water splitting, consisting of the oxygen evolution reaction (OER) and the hydrogen evolution reaction (HER), has been explored and used for decades. Noble metals are so far the most efficient electrocatalyst (*e.g.* iridium dioxide/ruthenium dioxide for the OER, and platinum for the HER) owing to their low overpotential and fast kinetics.[1–5] However, the high cost usually limits their large-scale applications. Therefore, it is necessary and urgent to design new efficient

electrocatalysts with low cost and high earth abundance, instead of noble metal-based catalysts. Moreover, in the present 2-compartment electrolyzer cells, an optimized anode in a suitable anode electrolyte and an optimized cathode in a suitable cathode electrolyte are operated, *e.g.* in a membrane configuration. Operation in a one-electrolyte configuration would require the presence of a catalyst that is able provide HER and OER activity.[6,7]

In this context, recently, layered double hydroxide materials (*e.g.* NiFe LDH, CoFe LDH, and NiCo LDH) have attracted intensive interest towards the OER.[8–13] However, the HER electrocatalytic activity is unsatisfactory, due to the poor conductivity and insufficient electrochemical active sites for this reaction. Oxygen vacancy engineering has been applied to promote OER and HER performances, owing to its beneficial effects on charge transfer and dissociation of water molecules.[13,14] The absence of oxygen ions changes the electronic structure of the surface and thus transforms a semiconductor into a metal-like conductor, combined with dangling bonds and gap states. Another effect is the generation of low coordination metals that leads to active sites of metal oxides/hydroxides.[1] Besides, altering the nature and density of oxygen vacancies in LDH materials exposes use of surface atoms.[15–17] For example,

[a]School of Chemistry and Chemical Engineering, Inner Mongolia Engineering and Technology Research Center for Catalytic Conversion and Utilization of Carbon Resource Molecules, Inner Mongolia University, 235 West University Street, Hohhot 010021, P. R. China. E-mail: wanglei@imu.edu.cn

[b]Advanced Coating Technology Research Center, National Institute of Advanced Industrial Science and Technology, Tsukuba Central 5, 1-1-1 Higashi, Tsukuba, Ibaraki 305-8565, Japan. E-mail: t-nakajima@aist.go.jp

[c]Key Laboratory of Materials Processing and Mold, Ministry of Education, Zhengzhou University, Zhengzhou 450002, P. R. China

[d]Department of Materials Science and Engineering WW4-LKO, University of Erlangen-Nuremberg, Martensstrasse 7, D-91058 Erlangen, Germany. E-mail: schmuki@ww.uni-erlangen.de

† Electronic supplementary information (ESI) available. See DOI: 10.1039/c9ta12768b

2490 | *J. Mater. Chem. A*, 2020, **8**, 2490–2497

This journal is © The Royal Society of Chemistry 2020

Wang and coworkers reported that exfoliation of bulk CoFe LDH into ultrathin LDH nanosheets through Ar/water plasma etching resulted in the formation of multiple vacancies, including O, Co, and Fe vacancies, for improving the intrinsic OER activity.[15,16] According to these treatments, the enhanced OER performances can be achieved for LDH-based catalysts in alkaline media. However, these electrocatalysts are still inert for the HER, let alone for overall water splitting. Therefore, it is still a challenge to achieve highly efficient HER activity of LDH-based materials, for developing bifunctional OER and HER electrocatalysts for overall one-pot water splitting.

We first perform a density functional theory (DFT) calculation to determine if the oxygen vacancies can influence the electronic structure of LDH and the surface adsorption energy of the reactants, and further the HER activity. Taking CoFe LDH material as an example, oxygen vacancies are constructed and Ce doping is considered and simulated by replacing O on the top surface. The optimized structures are shown in Fig. 1a. The HER activity is governed by the adsorption free energy of hydrogen (ΔG_{H*}).[1,18] For a fast proton/electron-transfer process and hydrogen release process, the ΔG_{H*} value should be close to zero. Fig. 1b shows that the $|\Delta G_{H*}|$ of CoFe LDH with oxygen vacancies (V-CoFe LDH) is 0.18 eV, which is much lower than that of CoFe LDH (0.55 eV). This indicates favorable H* adsorption kinetics on V-CoFe LDH for the HER. Besides, Ce insertion into CoFe LDH (Ce/CoFe LDH) exhibits a $|\Delta G_{H*}|$ value of 0.26 eV. Further oxygen vacancies provide a $|\Delta G_{H*}|$ value of 0.14 eV for V-Ce/CoFe LDH. This confirms that Ce doping and oxygen vacancies indeed can lower the energy barrier and facilitate the HER process, as well as enhance the HER activity.

Motivated by the promising predictions, in this work, we synthesize CoFe LDH with oxygen vacancy defects by a plasma etching strategy and establish it as a highly active HER catalyst in alkaline media. In contrast to the oxygen vacancy engineering, the phase transformation of CoFe LDH into CoFe$_2$O$_4$ occurs. Further, introduction of Ce leads to more active sites and improved electrical conductivity, resulting in a high efficiency of HER activity for V-Ce/CoFe LDH. The experimental results agree well with the DFT calculation, proving that the oxygen vacancy defects in CoFe LDH or Ce/CoFe LDH lead to an outstanding HER performance. More importantly, the CoFe LDH‖V-Ce/CoFe LDH is capable of overall water splitting with a cell voltage as low as 1.65 V at a current density of 10 mA cm^{-2}

and remarkable long-term stability. These findings provide a simple but feasible pathway for the design of advanced LDH materials for energy conversion devices.

Results and discussion

Fig. 2a illustrates the synthesis of V-CoFe LDH and V-Ce/CoFe LDH. First, CoFe LDH is prepared by a hydrothermal method in an aqueous solution containing Co(NO$_3$)$_2$·6H$_2$O and Fe(NO$_3$)$_3$·9H$_2$O with a molar ratio of Co : Fe = 1 : 1. The CoFe LDH is composed of 2 dimensional (2D) nanosheets with a thickness of 40–60 nm (Fig. S1a and S2†). Transmission electron microscopy (TEM) images (Fig. S3†) present the lattice fringes with distances of 0.26 nm, 0.23 nm, and 0.15 nm, matching well with the (012), (015), and (110) planes of CoFe LDH, respectively. Subsequently, the CoFe LDH was subjected to plasma etching to synthesize the defected CoFe LDH (denoted as V-CoFe LDH). As shown in Fig. S1b,† many pores and small fragments are observed. TEM images present a nanosheet structure consisting of small nanocrystallites, and these small nanocrystallites are surrounded by amorphous shells (Fig. S4†). Atomic force microscopy (AFM) images show that the height of V-CoFe LDH is approximately 5 nm, which is around 10 times thinner compared to a single layer of LDH (Fig. S2†). This indicates that LDH could be exfoliated, in line with the results reported by Wang et al.[17] We further induced Ce doping into the LDH as shown in Fig. 2a. No obvious change in morphology is observed compared to the CoFe LDH (Fig. 2b, S1c, and S5†). Further N$_2$ plasma treatment leads to abundant amorphous sites and defects detected in V-Ce/CoFe LDH (Fig. 2h and S6†), which are similar to the V-CoFe LDH. The elemental mapping images from energy dispersive X-ray spectroscopy (EDS) confirm a homogeneous distribution of Co, Fe, Ce, and O species (Fig. 2j). Closely resembling the V-CoFe LDH, the thickness of V-Ce/CoFe LDH nanosheets decreases to ∼5 nm after the etching process (Fig. S7†). Combined with the TEM results, abundant defects and amorphous phases caused by the plasma etching might induce a higher surface area and more active sites, facilitating the electron transfer and OH$^-$/H$_2$O adsorption, subsequently further promoting the HER activity.

The crystalline structures of CoFe LDH and Ce/CoFe LDH without and with N$_2$ plasma etching were investigated by X-ray diffraction (XRD). The corresponding powders (Fig. S8†) were examined, as the low amount of LDHs growing on nickel foam (NF) led to weak signals in XRD spectra. Fig. 3a shows that two phases composed of CoFe LDH (JCPDS 50-0235) and CoFe$_2$O$_4$ (JCPDS 01-1121) exist in the LDH powders.[19] Through N$_2$ plasma etching treatment, all diffraction peaks that can be assigned to (00l) (l = 3, 6 and 9), (015) and (018) in LDH decrease, while the CoFe$_2$O$_4$ remains unaffected by it. The different plasma etching times of XRD patterns were further investigated as shown in Fig. S9a.† With increasing etching time, the diffraction peaks for the LDH finally disappear after 120 s. To probe the details of phase transformation, 2D XRD mappings were conducted as shown in Fig. S9b.† The (00l) Debye-rings are clearly observed but disappear after 120 s, indicating that this structural transformation of LDH does not derive from a deformation of crystal
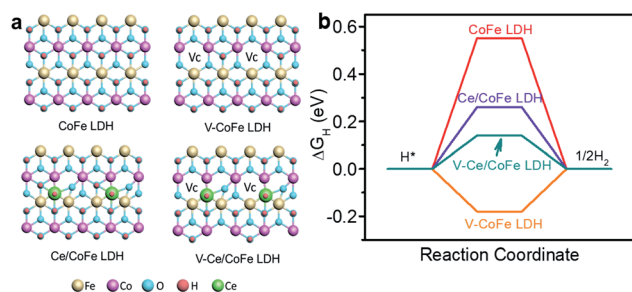

Fig. 1 (a) Structures and (b) free energy diagram of the HER over CoFe LDH, V-CoFe LDH, Ce/CoFe LDH, and V-Ce/CoFe LDH.
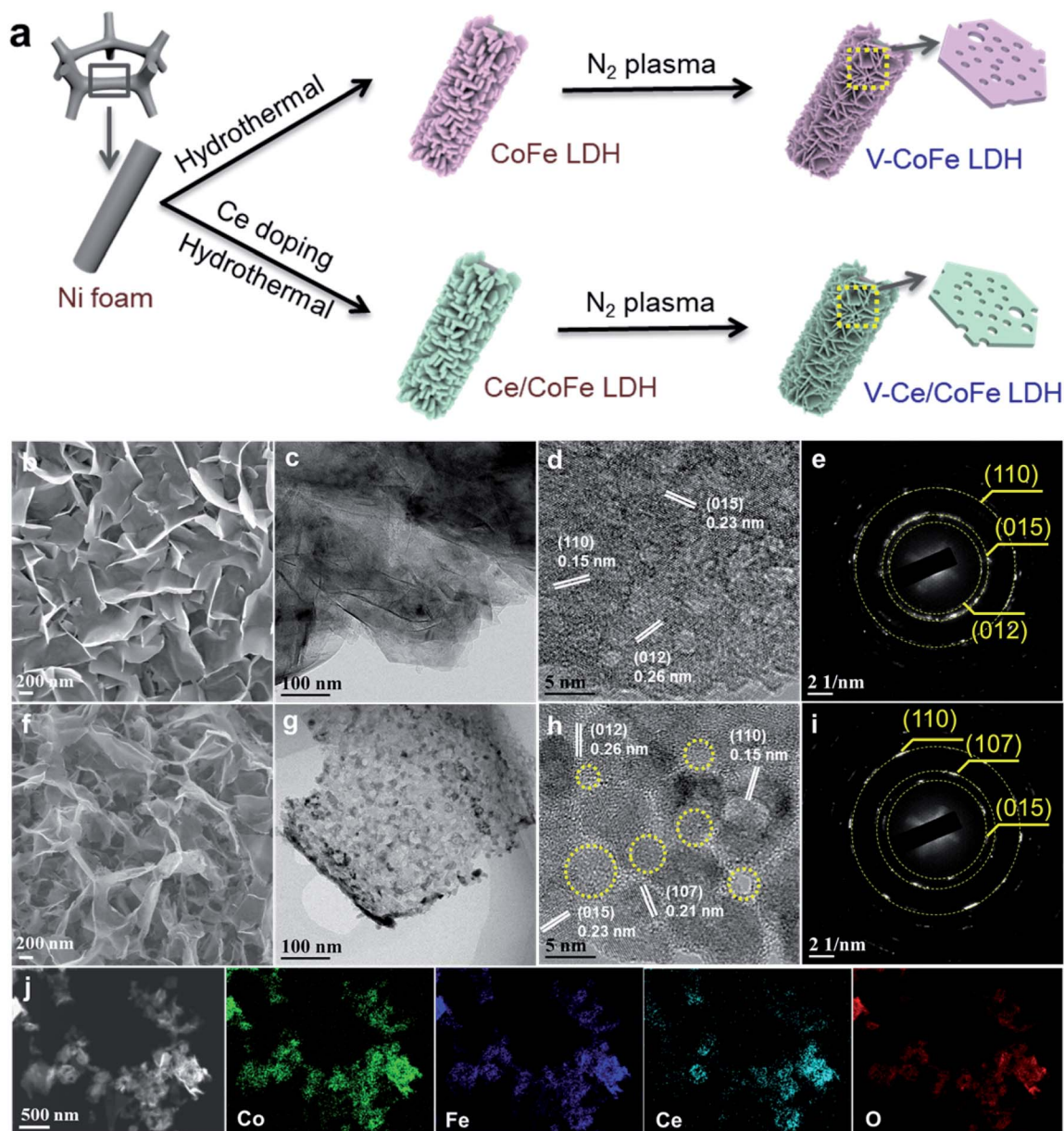
Fig. 2 (a) Schematic illustration of synthesis of V-CoFe LDH and V-Ce/CoFe LDH; (b) SEM image, (c and d) TEM images, and (e) SAED pattern of Ce/CoFe LDH; (f) SEM image, (g and h) TEM images, and (i) SAED pattern of V-Ce/CoFe LDH; (j) TEM-EDS mapping images of V-Ce/CoFe LDH.

orientation but from the shortening crystal coherent length. By using the collected X-ray diffraction of 2D mapping in the range of $\beta = -22°$ to $22°$ (β: Debye-ring direction) for the LDH, we evaluate the lattice strain of LDH crystals based on William–Hall analysis (Fig. S9c and d†). The lattice strain (ε) can be evaluated using the slope of a plot of $F_{hkl} \cos \theta$ versus $4 \sin \theta$ based on the following equation:[20]

$$F_{hkl} \cos \theta / \lambda = k\lambda/D + 4\varepsilon \sin \theta \quad (1)$$

where F_{hkl} is the full width at half-maximum intensity of diffraction peaks, θ is the diffraction angle, λ is the X-ray wavelength (CuKα: 1.5405 Å), D is the crystallite size, and k is Scherrer's constant (0.94). Both CoFe- and Ce/CoFe LDHs tend

to increase the lattice strain with increasing plasma etching time, and the larger strain is introduced in the Ce/CoFe LDH compared to the CoFe LDH owing to Ce doping. This could be also related to the fragmented crystallite sizes of CoFe and Ce/CoFe LDHs (Fig. S4 and S6†). Different from previous studies,[15–17] except for the formation of defects, phase transformation is possibly one of the reasons for the adsorption of molecular H_2O and the enabled water splitting reaction.

X-ray photoelectron spectroscopy (XPS) measurements were performed to probe chemical valence states in the samples. In the Co 2p spectra (Fig. S10 and S11†), the peaks at 780.9 eV and 782.0 eV are ascribed to the Co^{3+} and Co^{2+}. The Co^{3+} is partially reduced to Co^{2+}, producing oxygen vacancies after plasma etching. The Fe 2p spectrum shows two peaks at 713.9 eV and

2492 | J. Mater. Chem. A, 2020, 8, 2490–2497

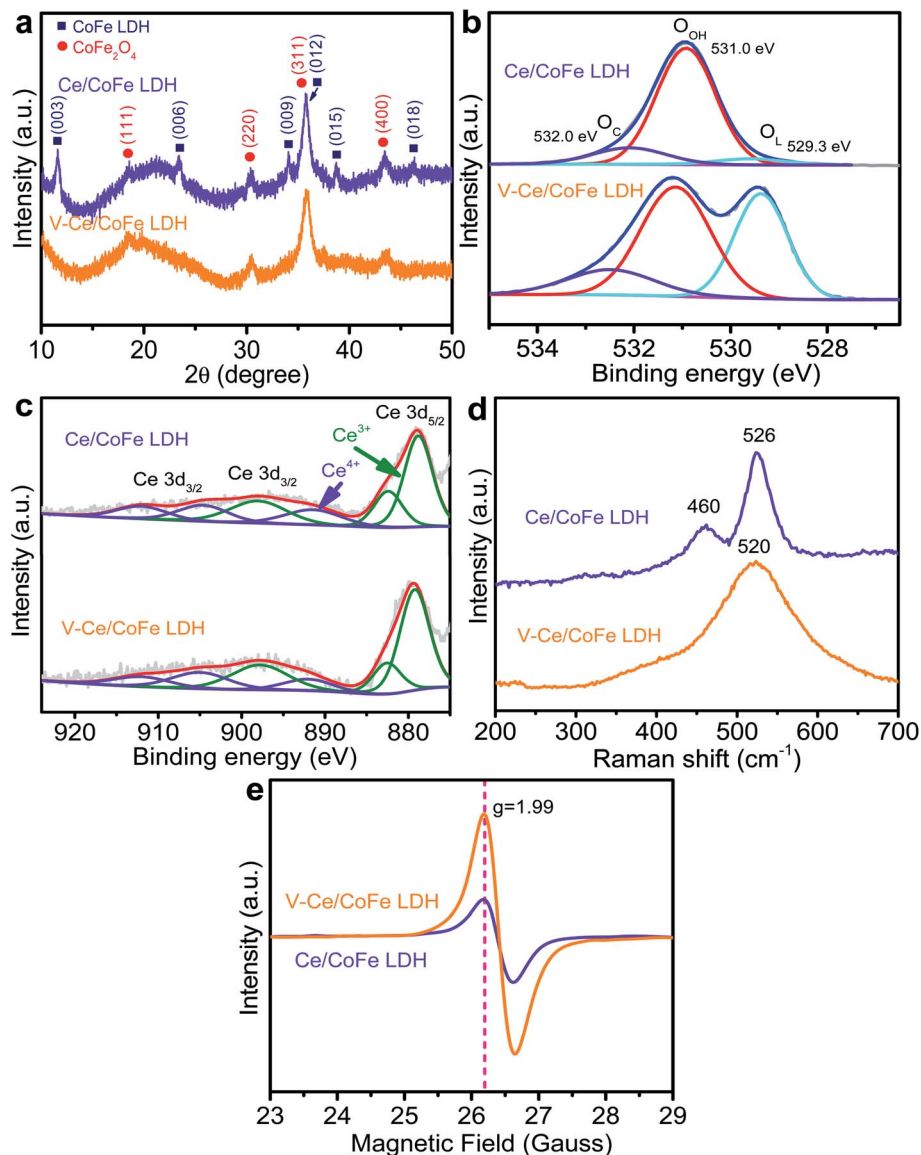This journal is © The Royal Society of Chemistry 2020

Fig. 3 (a) XRD patterns of Ce/CoFe LDH and V-Ce/CoFe LDH powders; (b) O 1s and (c) Ce 3d XPS spectra, (d) Raman spectra, and (e) EPR results of Ce/CoFe LDH and V-Ce/CoFe LDH.

724.1 eV, indicating the presence of Fe^{3+} in the CoFe LDH. Compared to the pristine LDH, a new peak around 707.2 eV in Fe 2p of V-CoFe LDH (and V-Ce/CoFe LDH) appears (Fig. S10b and S11b†), which can be ascribed to metallic Fe. Additionally, there is an obvious peak shift toward low binding energies after the plasma treatment. This suggests that the electronic structure in LDH becomes electron-enriched after etching.[13,21] In Fig. 3b, the O 1s peak can be attributed to the metal–oxygen (M−O) bond in the lattice (529.3 eV), hydroxide bond (O–H) in the material (531.0 eV), and chemisorbed oxygen (O–O) on and within the surface (532.0 eV).[15] There is a negligible change without or with plasma treatment in LDH (Fig. 3b and S10†). However, a remarkable difference is detected for both CoFe- and Ce/CoFe LDHs after plasma etching (Fig. S10c and S11c†). Namely, the O–H bond has a minute change before and after plasma treatment, while the intensities of M−O and absorbed

O–O signals are increased after plasma etching. Liu *et al.*[21] demonstrated that a LDH layer with tensile strain induced by ball-milling facilitated oxygenated intermediate adsorption. In our case, the increased O–O signal indicates an enhanced binding strength of the plasma-etched LDH surface to oxygenated intermediates.[13,22,23] The M−O bond can be ascribed to the transformation of metal-hydroxide into metal oxy-hydroxide. Additionally, the coexistence of Ce^{3+} and Ce^{4+} is evidenced in the Ce 3d XPS spectra (Fig. 3c).

Raman spectroscopy was further used to investigate plane vibration modes of corresponding materials, and it reveals a clear difference for samples without and with plasma etching treatments. As shown in Fig. 3d and S12,† the bands at 460 cm^{-1} and 526 cm^{-1} attributed to the metal–OH translation mode change to a broadened peak at 516–520 cm^{-1} after exfoliation, accompanied by a red shift, resulting from phonon

softening induced by tensile strain.[21,24,25] Based on d band theory, lattice strain is able to change the surface d bandwidth, which moves up or down the d band center to maintain a constant band filling state.[21] The increased lattice strain in CoFe LDH is expected to upshift the d band center towards the Fermi level, leading to a less filled anti-bonding state and narrow band gap. Mott–Schottky measurements were carried out to determine the flat-band potential (E_{fb}) of CoFe LDH. It demonstrates that the E_{fb} of V-CoFe LDH is shifted from CoFe LDHs (Fig. S13†), suggesting a better electron conductivity and a high intrinsic HER activity of plasma treated CoFe LDH. Furthermore, electron paramagnetic resonance (EPR) spectroscopy (Fig. 3e and S14†) demonstrates that the V-CoFe LDH and V-Ce/CoFe LDH have more defects in the structure, and the signal ($g = 1.99$) reveals structural defects from oxygen vacancies, which is in accordance with a report of Zhao et al.[13]

Fig. 4a shows the linear sweep voltammetry (LSV) results of the corresponding electrocatalysts in 1 M KOH for their electrocatalytic HER activities. Various plasma power densities, plasma times, and Ce contents were optimized with respect to the best HER performance (Fig. S15 and S16†). In Fig. 4a, the IR-corrected polarization curve of the V-CoFe LDH exhibits a lower overpotential compared to the pristine CoFe LDH. The optimum overpotential at 10 mA cm^{-2} is 95 mV lower than that of the pristine one (194 mV), indicating a significantly improved HER performance for plasma etched samples. Ce/CoFe LDH displays an overpotential of 156 mV at 10 mA cm^{-2}. When the Ce/CoFe LDH was treated in N$_2$ plasma, the overpotential further decreases to 73 mV at 10 mA cm^{-2}, close to the Pt/C electrode (30 mV), which is one of the best results for the LDH-based electrocatalysts. Moreover, a much smaller slope (69 mV dec^{-1}) of the Tafel plot is obtained for the V-Ce/CoFe LDH (Fig. 4b), suggesting an enhanced HER activity due to Ce doping, oxygen vacancies, and phase transformation. These results match well with the DFT calculation as shown in Fig. 1 – demonstrating a fast hydrogen release process to facilitate the
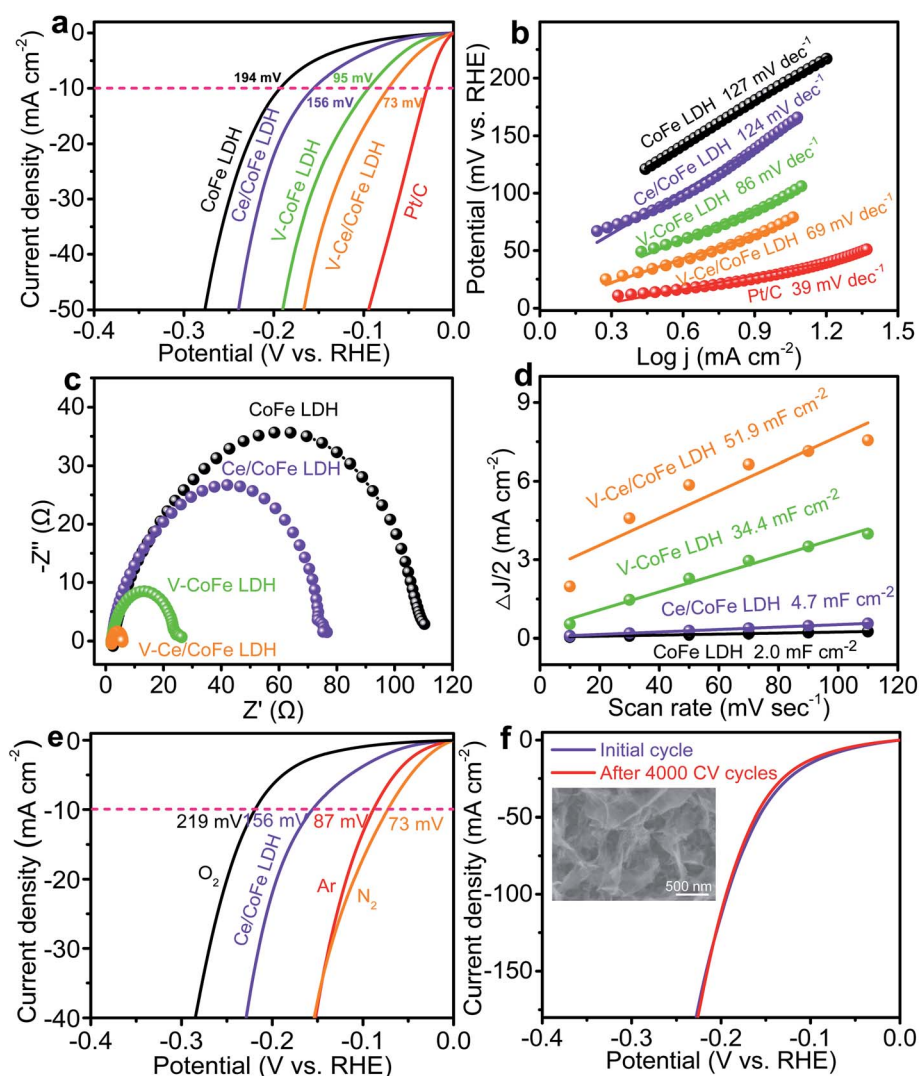

Fig. 4 HER performances of CoFe LDH, V-CoFe LDH, Ce/CoFe LDH, and V-Ce/CoFe LDH in 1 M KOH electrolyte: (a) IR-corrected polarization curves; (b) Tafel plots; (c) EIS; (d) capacitance current as a function of scan rate; (e) IR-corrected polarization curves of Ce/CoFe LDH plasma treated in various atmospheres; (f) IR-corrected polarization curves of V-Ce/CoFe LDH initially and after 4000 CV cycles.

2494 | J. Mater. Chem. A, 2020, 8, 2490–2497

This journal is © The Royal Society of Chemistry 2020

HER process for the LDH layer after doping and plasma treatments.

To figure out the nickel foam effect and confirm the advantage of plasma etching treatment, Ce/CoFe LDH powder was prepared on carbon cloth for comparison. The V-Ce/CoFe LDH powder on carbon cloth has a lower overpotential than the pristine Ce/CoFe LDH powder (Fig. S17†), providing a strong evidence that the plasma etching strategy is indeed beneficial for promoting the HER performance. Additionally, it indicates that the existence of $CoFe_2O_4$ has a positive effect on HER activity.

Electrochemical impedance spectroscopy (EIS) was carried out to obtain more insights into the electron-transfer kinetics of the HER. Fig. 4c shows that V-Ce/CoFe LDH has the smallest charge transfer resistance than other electrodes, implying favorable reaction kinetics. To explore the intrinsic catalytic activities of these catalysts, an electrochemical double-layer capacitance (C_{dl}) approach was applied to estimate the electrocatalytic active surface area (ECSA) from cyclic voltammetry curves at various scan rates over a small potential range (Fig. S18†). Notably, the V-Ce/CoFe LDH electrode possesses the largest C_{dl} of 51.9 mF cm^{-2} compared to those of V-CoFe LDH (34.4 mF cm^{-2}), Ce/CoFe LDH (4.7 mF cm^{-2}), and CoFe LDH (2.0 mF cm^{-2}) shown in Fig. 4d, showing indeed that a larger ECSA of V-Ce/CoFe LDH allows more exposed active sites to promote HER performance.

To rule out any direct plasma atmospheric effect on HER activity, Ce/CoFe LDH samples were treated in different plasma atmospheres (e.g. Ar and O_2), and the corresponding LSV curves are shown in Fig. 4e. Clearly, the CoFe LDH treated in Ar or N_2 plasma exhibits the improved HER activity, and even close values of overpotentials of 87 mV and 73 mV at 10 mA cm^{-2}, respectively, while the sample treated in an oxygen atmosphere displays an increased overpotential (219 mV). XPS shows a very weak N 1s peak (Fig. S19†) due to the short nitrogen plasma time (at 500 W for 10 s). N is possibly absorbed only on the top surface, so we exclude the effect of N doping in the LDH, but the oxygen effect points again to oxygen vacancies as the most important factor. We also measured the HER activity in neutral media (Fig. S20†). Clearly, the V-Ce/CoFe LDH exhibits the best HER performance (212 mV at 10 mA cm^{-2}) among them.

Besides, a thick CoFe LDH material on nickel foam was prepared according to reported literature (Fig. S21†)[26] and then treated under the same plasma conditions; the overpotential is reduced from 208 mV (pristine) to 170 mV (Fig. S22†). This further demonstrates that the plasma etching does promote the HER activity. However, this thick CoFe LDH did not have a good long-term stability owing to dissolution of LDH in the electrolyte. Additionally, a thick layer is more easily etched off during the plasma process, which leads to a relatively lower HER performance compared to the LDH material we used in this work. Thus, we choose a thin CoFe LDH layer with a strong adhesion to the substrate for an excellent electrocatalytic performance.

To identify if the plasma etching approach can be applied for other LDH materials, NiFe- and NiCo LDHs were grown on nickel foams and then treated under the same conditions. They also exhibit the enhanced HER performances after plasma etching (Fig. S23†). Furthermore, the V-Ce/CoFe LDH was subjected to CV measurements for 4000 cycles, and the polarization curve has only a tiny change (Fig. 4f), suggesting a good long-term stability. No significant changes in morphology in SEM (inset of Fig. 4f) and TEM images (Fig. S24†) are observed after CV, and the single nanosheet and defects still exist, further confirming a good durability. In the XPS spectra (Fig. S25†), Co, Ni, and Ce are detected, while the O 1s peak after cycling can be mainly attributed to the hydroxide bond (M−OH), indicating that the structure has changed from metal oxy-hydroxides to metal hydroxides after the HER. This phenomenon has also been observed in other studies.[27,28] Based on the results above, in our case, the HER performance of V-Ce/CoFe LDH is better than or comparable to that of reported non-noble CoFe-based electrocatalysts (Table S1†). Therefore, this strategy clearly has a positive effect on the improvement of the HER electrocatalytic activity of LDH-based catalysts.

Finally, inspired by the superior HER performance of the V-Ce/CoFe LDH in alkaline media, we used the optimized CoFe LDH/V-Ce/CoFe LDH as the anode and cathode to construct a two-electrode electrolyzer for overall water splitting in a KOH electrolyte. The polarization curve in Fig. 5a shows that the CoFe LDH‖V-Ce/CoFe LDH cell reaches a current density of 10 mA cm^{-2} at an overpotential of 1.65 V. Such a performance is
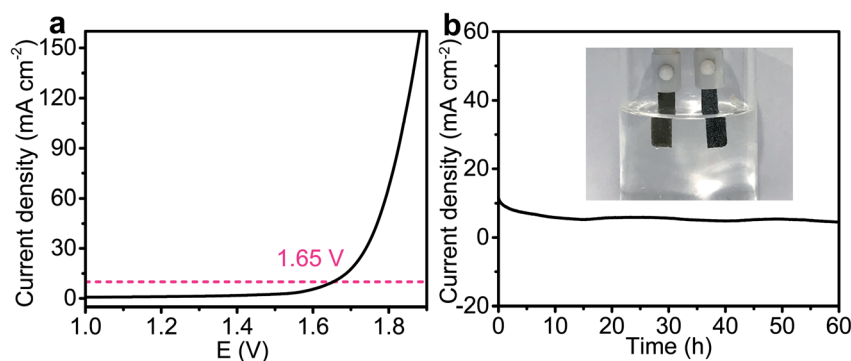

Fig. 5 (a) Performance of the full water-splitting device using the CoFe LDH as the anode and V-Ce/CoFe LDH as the cathode; (b) chronoamperometric curve of CoFe LDH‖V-Ce/CoFe LDH for full water splitting with an overpotential of 10 mA cm^{-2} for 60 h. The inset of b shows the optical photograph of generation gases.

This journal is © The Royal Society of Chemistry 2020

J. Mater. Chem. A, 2020, **8**, 2490–2497 | **2495**

better than the values reported for CoFe-based electrocatalysts. Furthermore, the CoFe LDH‖V-Ce/CoFe LDH cell displays an excellent electrochemical durability with no noticeable decrease at a constant applied potential of 1.65 V for 60 h (Fig. 5b). The generated O_2 and H_2 were further measured quantitatively, and the ratio is close to 1 : 2 (Fig. S26†).

In this work, the exfoliation process leads to an increase of reactive sites in the holes with more dangling bonds and lower coordination numbers. The increasing number of reactive sites from higher specific surface area further leads to the rearrangement of the electronic configuration. Based on the first-principle calculation and experimental results, the high HER activity of V-Ce/CoFe LDH originates from the synergistic effects of large ECSA, oxygen vacancies, and improved electrical conductivity, facilitating fast charge transfer induced by the plasma etching process.[29] More importantly, phase transformation processes occurred during this treatment (this effect is the first time reported in this work). For the CoFe- and Ce/CoFe LDH powders, two phases of CoFe LDH and $CoFe_2O_4$ both exist, and the CoFe LDH transforms into $CoFe_2O_4$ with increasing plasma time. For the CoFe LDH grown on nickel foam, less $CoFe_2O_4$ is possibly formed, but with plasma etching, the LDH phase is changed to an oxy-hydroxide phase as confirmed by XPS and Raman analysis (Fig. S10c, S11c, and S12†). Both CoFe LDH and Ce/CoFe LDH tend to increase the lattice strain with increasing plasma etching time, and a larger strain is introduced in the Ce/CoFe LDH as compared to the CoFe LDH. Therefore, it is deduced that the plasma etching strategy not only induces vacancies and defects, but can also induce beneficial phase transformations.

Conclusions

In summary, we synthesize CoFe LDH with oxygen-vacancy defects by nitrogen plasma etching and demonstrate the resulting material as a highly active HER catalyst in alkaline media. The as-prepared V-CoFe LDH was further modified with Ce doping. It maintains the two-dimensional nanosheet structure but with enlarged ECSA and active sites, and with better electrical conductivity. During the plasma etching, a phase transformation of CoFe LDH into $CoFe_2O_4$ further improves the electrocatalytic reaction kinetics. The resulting V-Ce/CoFe LDH shows a high activity (73 mV at 10 mA cm^{-2}) and a good durability in 1 M KOH electrolyte. Such CoFe LDH‖V-Ce/CoFe LDH is capable of overall water splitting with a cell voltage as low as 1.65 V at 10 mA cm^{-2} and outstanding long-term stability. Our work provides a new strategy to the realization of LDH-based electrocatalysts with excellent HER performances.

Conflicts of interest

There are no conflicts to declare.

Acknowledgements

Notes and references

1 L. Han, S. Dong and E. Wang, *Adv. Mater.*, 2016, **28**, 9266–9291.

2 J. Liu, D. Zhu, Y. Zheng, A. Vasileff and S.-Z. Qiao, *ACS Catal.*, 2018, **8**, 6707–6732.

3 V. Vij, S. Sultan, A. M. Harzandi, A. Meena, J. N. Tiwari, W.-G. Lee, T. Yoon and K. S. Kim, *ACS Catal.*, 2017, 7, 7196–7225.

4 Z. Chen, X. Duan, W. Wei, S. Wang and B.-J. Ni, *J. Mater. Chem. A*, 2019, 7, 14971–15005.

5 J. F. Callejas, C. G. Read, C. W. Roske, N. S. Lewis and R. E. Schaak, *Chem. Mater.*, 2016, **28**, 6017–6044.

6 R. Yang, Y. Zhou, Y. Xing, D. Li, D. Jiang, M. Chen, W. Shi and S. Yuan, *Appl. Catal., B*, 2019, **253**, 131–139.

7 Y. Li, M. Lu, Y. Wu, H. Xu, J. Gao and J. Yao, *Adv. Mater. Interfaces*, 2019, **6**, 1900290.

8 G. Rajeshkhanna, T. I. Singh, N. H. Kim and J. H. Lee, *ACS Appl. Mater. Interfaces*, 2018, **10**, 42453–42468.

9 T. Zhang, L. Hang, Y. Sun, D. Men, X. Li, L. Wen, X. Lyu and Y. Li, *Nanoscale Horiz.*, 2019, **4**, 1132–1138.

10 P. F. Liu, S. Yang, B. Zhang and H. G. Yang, *ACS Appl. Mater. Interfaces*, 2016, **8**, 34474–34481.

11 X. Wang, Y. Yang, L. Diao, Y. Tang, F. He, E. Liu, C. He, C. Shi, J. Li, J. Sha, S. Ji, P. Zhang, L. Ma and N. Zhao, *ACS Appl. Mater. Interfaces*, 2018, **10**, 35145–35153.

12 H. Xu, B. Wang, C. Shan, P. Xi, W. Liu and Y. Tang, *ACS Appl. Mater. Interfaces*, 2018, **10**, 6336–6345.

13 M. Asnavandi, Y. Yin, Y. Li, C. Sun and C. Zhao, *ACS Energy Lett.*, 2018, **3**, 1515–1520.

14 L. Xu, Q. Jiang, Z. Xiao, X. Li, J. Huo, S. Wang and L. Dai, *Angew. Chem., Int. Ed.*, 2016, **55**, 5277–5281.

15 Y. Wang, Y. Zhang, Z. Liu, C. Xie, S. Feng, D. Liu, M. Shao and S. Wang, *Angew. Chem., Int. Ed.*, 2017, **56**, 5867–5871.

16 R. Liu, Y. Wang, D. Liu, Y. Zou and S. Wang, *Adv. Mater.*, 2017, **29**, 1701546.

17 Y. Wang, C. Xie, Z. Zhang, D. Liu, R. Chen and S. Wang, *Adv. Funct. Mater.*, 2018, **28**, 1703363.

18 S. Niu, W.-J. Jiang, Z. Wei, T. Tang, J. Ma, J.-S. Hu and L.-J. Wan, *J. Am. Chem. Soc.*, 2019, **141**, 7005–7013.

19 A. E. Arrassi, Z. Liu, M. V. Evers, N. Blanc, G. Bendt, S. Saddeler, D. Tetzlaff, D. Pohl, C. Damm, S. Schulz and K. Tschulik, *J. Am. Chem. Soc.*, 2019, **141**, 9197–9201.

20 V. Mote, Y. Purushotham and B. Dole, *Journal of Theoretical and Applied Physics*, 2012, **6**, 6.

2496 | *J. Mater. Chem. A*, 2020, **8**, 2490–2497

This journal is © The Royal Society of Chemistry 2020

21 D. Zhou, S. Wang, Y. Jia, X. Xiong, H. Yang, S. Liu, J. Tang, J. Zhang, D. Liu, L. Zheng, Y. Kuang, X. Sun and B. Liu, *Angew. Chem.*, 2019, **131**, 746–750.

22 H. B. Tao, L. Fang, J. Chen, H. B. Yang, J. Gao, J. Miao, S. Chen and B. Liu, *J. Am. Chem. Soc.*, 2016, **138**, 9978–9985.

23 A. Tamilselvan, S. Balakumar, M. Sakar, C. Nayek, P. Murugavel and K. Saravana Kumar, *Dalton Trans.*, 2014, **43**, 5731–5738.

24 V. R. R. Cunha, P. A. D. Petersen, M. B. Goncalves, H. M. Petrilli, C. Taviot-Gueho, F. Leroux, M. L. A. Temperini and V. R. L. Constantino, *Chem. Mater.*, 2012, **24**, 1415–1425.

25 G. Tsoukleri, J. Parthenios, K. Papagelis, R. Jalil, A. C. Ferrari, A. K. Geim, K. S. Novoselov and C. Galiotis, *Small*, 2009, **5**, 2397–2402.

26 R. Yang, Y. Zhou, Y. Xing, D. Li, D. Jiang, M. Chen, W. Shi and S. Yuan, *Appl. Catal., B*, 2019, **253**, 131.

27 J. Huang, Q. Shang, Y. Huang, F. Tang, Q. Zhang, Q. Liu, S. Jiang, F. Hu, W. Liu, Y. Luo, T. Yao, Y. Jiang, Z. Pan, Z. Sun and S. Wei, *Angew. Chem., Int. Ed.*, 2016, **55**, 2137–2141.

28 Q. Zhang, S. Zhang, Y. Tian and S. Zhan, *ACS Sustainable Chem. Eng.*, 2018, **6**, 15411–15418.

29 Z. Yuan, S.-M. Bak, P. Li, Y. Jia, L. Zheng, Y. Zhou, L. Bai, E. Hu, X.-Q. Yang, Z. Cai, Y. Sun and X. Sun, *ACS Energy Lett.*, 2019, **4**, 1412–1418.

This journal is © The Royal Society of Chemistry 2020

J. Mater. Chem. A, 2020, **8**, 2490–2497 | **2497**